Dynamical control techniques to generate arbitrary qutrit populations in superconducting transmon qubits

Author: Ivan Alsina Ferrer
Facultat de Física, Universitat de Barcelona, Diagonal 645, 08028 Barcelona, Spain.

Advisors: Pol Forn-Díaz (IFAE), Sofyan Iblisdir (UB)

Transmon devices have shown suitable features to work as qubits and thus serve as a unit of information in quantum computers. However, a recent interest in keeping the higher dimensions of the Hilbert space compels the search of techniques to exploit them. In this paper, the evolution of the four first quasi-harmonic energy states of the transmon device are considered, in order to discuss and compare four techniques to prepare 3-dimensional states.

I. INTRODUCTION

In recent years, a substantial amount of work has been performed to develop functional quantum computers. These promise to deliver the unique features of the quantum world so as to efficiently solve problems very difficult to tackle with classical computers.

The basic unit of quantum computation is the quantum bit, or *qubit* [1]. Nevertheless, the consideration of systems with more than two states allows for more local operations and less entangling gates might be required for the performance of a specific computation [2]. This makes way for the *qudit* formalism, where $d > 2$ levels of a quantum state are considered in order to model the quantum system and develop quantum gates and algorithms. This is especially relevant when the physical realization relies on a system susceptible to be measured in more than two states, such as the superconducting quantum circuits like the one used in this work. Other examples include quantum dots [3], harmonic oscillator states [4] and the rotational and vibrational states of a molecule [5].

The superconducting transmon device is based on a capacitively shunted Josephson junction that can be portrayed as an artificial atom whose energy levels E_k ($k \geq 0$) can be approximated by [6]

$$E_k \approx -E_J + \sqrt{8E_C E_J}\left(k + \frac{1}{2}\right) - \frac{E_C}{12}\left(6k^2 + 6k + 3\right), \tag{1}$$

where $E_C = e^2/2C$ is the charging energy (being C being the shunting capacitance), and $E_J = I_c\Phi_0/2\pi$ is the Josephson energy (I_c is the critical current and $\Phi_0 = h/2e$ is the quantum of flux in the junction) [7]. This leads to a deviation in the harmonic oscillator energy structure, that takes form in a difference of 0-1 and 1-2 transition energies, called anharmonicity (α):

$$\hbar\alpha \equiv (E_2 - E_1) - (E_1 - E_0) \approx -E_C. \tag{2}$$

This allows to externally act on a specific transition.

In the present work, different techniques for the preparation of arbitrary 3-level states (*qutrit*) are presented and compared. To do so, the ground state $|0\rangle$ and the three first excited states $|1\rangle$, $|2\rangle$, $|3\rangle$ are considered. Different techniques are explored, with the purpose of preparing states with wave functions $|\Psi\rangle$ in the 4-dimensional Hilbert space containing a desired mix of populations P_0, P_1 and P_2 in each state. The upper state population, P_3, solely an indicator that should remain small as a sign of correct operation of our protocols.

Since the characteristic population decay time T_1 has been measured to be above 10 µs, simulations will be restricted to pulses below 120 ns and considered unaffected by decoherence. Therefore, the Schrödinger equation

$$i\frac{\mathrm{d}}{\mathrm{d}t}|\Psi\rangle = \mathcal{H}|\Psi\rangle, \tag{3}$$

is in each case numerically solved to find the evolution of a state $|\Psi\rangle$ that is always regarded to be $|\Psi(t=0)\rangle = |0\rangle$ at the beginning of the evolution due to a previous relaxation of the system. To do so, the QuTiP package [8] has been used on a system whose parameters are presented in table A.I.

II. DRIVE IN N-DIMENSIONAL SYSTEMS

The coupling of a qubit, provided with a ground state ($|0\rangle$) and excited state ($|1\rangle$), with a microwave field that oscillates at drive frequency ω_d can be described by:

$$\mathcal{H} = \frac{\hbar\omega_q}{2}\sigma_z + \hbar\Omega\cos(\omega_d t)\sigma_x, \tag{4}$$

where ω_q is the qubit frequency, i.e. the energy difference between the states in units of $\hbar$, and σ_x, σ_z are the Pauli matrices. Ω is the Rabi frequency: $\Omega = \hbar^{-1}\mathbf{d}\cdot\mathbf{E}_0$, with $\mathbf{d}$ the transition dipole moment and $\mathbf{E}_0$ the field amplitude. As a result, the probability of a system, initially prepared in the ground state to be measured in the excited state, P_1, is given by the Rabi formula [9]:

$$P_1(t) = \frac{\Omega^2}{\Delta\omega^2 + \Omega^2}\sin^2\left(\frac{\sqrt{\Delta\omega^2 + \Omega^2}}{2}t\right), \tag{5}$$

$\Delta\omega \equiv \omega_q - \omega_d$ being the drive detuning. The so-called π-pulse is such that the state $|1\rangle$ is fully populated at the end of the pulse.

The pulse $\mathcal{E}$ supposed to act on the qutrit system is

$$\mathcal{E}(t) = \Omega(t)\cos\left(\omega_d t + \Phi(t)\right), \tag{6}$$

with a time-dependent Rabi frequency $\Omega(t)$ and phase $\Phi(t)$. The Hamiltonian for the qutrit system is extended with respect to that of the qubit given in Eq. (4):

$$\mathcal{H} = \hbar\sum_{i=1}^{3}\omega_{0,i}\Pi_i + \hbar\sum_{i<j}^{3} g_{ij}\Omega\cos^{a_{ij}}(\omega_d t + \Phi)\Pi_{ij}, \tag{7}$$

where $\hbar\omega_{0,i}$ denotes the energy difference between the 0^{th} and the i-th energy level, Π_i and Π_{ij} are the projectors $|i\rangle\langle i|$ and $(|i\rangle\langle j| + |j\rangle\langle i|)$, respectively, a_{ij} is 2 if $j - i = 2$ –referring to a two-photon transition– or 1 otherwise. The coupling strengths g_{ij} corresponding to correlative energy levels are given by [6]

$$g_{j,j+1} \approx \sqrt{\frac{j+1}{2}}\left(\frac{E_J}{8E_C}\right)^{1/4}. \tag{8}$$

One-photon transitions between levels with the same parity, e.g. transition 0-2, are approximately forbidden [21] and not considered. However, two-photon mechanisms become dominant and occur at a frequency $\omega_{02}/2$ [10]. The coupling strength of this mechanism is here estimated to be $g_{02} \approx g_{01}/20$ [6] and contributes only as a small interfering process with negligible effect in our calculations. As for the third excited state, g_{03} is taken as $g_{01}/10$ [6], and the value g_{13} is taken to equal g_{02}, being a similarly weak two-photon process at $\omega_{13}/2$.

When the Hamiltonian of several levels is considered, the Rabi formula in (5) does not hold. In spite of that, it still shows that a pulse resonant with a specific transition produces out-of-resonance excitations of the other transitions, as can be seen in figure 1. This effect can be mitigated by applying pulses of small magnitude Ω.

III. EXISTING PROTOCOLS

A. DRAG protocol

A widely used protocol to generate the 0-1 rotation and purify the $|1\rangle$-state population of the qubit is the Derivative Removal by Adiabatic Gate (DRAG) [11, 12]. This protocol aims to analytically cancel the leakage of probability density towards the second excited state. A pulse with shape

$$\mathcal{E}(t) = \mathcal{E}_x(t)\cos\omega_d t + \mathcal{E}_y(t)\sin\omega_d t, \quad 0 \le t \le t_g \tag{9}$$

is suggested, where t_g is the gate time, $\mathcal{E}_x$ and $\mathcal{E}_y$ are independent quadrature controls, and the drive frequency ω_d is also time-dependent.

The conditions

$$\mathcal{E}_y(t) = -\frac{1}{\alpha}\frac{\mathrm{d}\mathcal{E}_x}{\mathrm{d}t} \quad \text{and} \quad \delta(t) = \frac{\lambda^2 - 4}{4\alpha}\mathcal{E}_x^2(t), \tag{10}$$

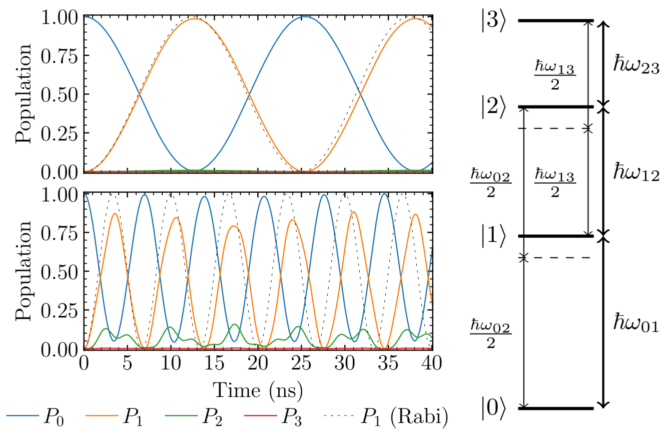

FIG. 1: State population under a pulse in resonance with the 0-1 transition ($\omega_d = \omega_{01}$) under a flat envelope of $\Omega = 2\pi \times 40\,\text{MHz}$ (top) and $\Omega = 2\pi \times 150\,\text{MHz}$ (bottom), with $\Phi = 0$. The population corresponding to the two-level Rabi formula of (5) in resonance ($\Delta\omega = 0$) is plotted in a thin dashed line. Right: Energy-level diagram of the transmon superconducting device, including one-photon and two-photon transitions. $\hbar\omega_{03}$ has been omitted for the sake of clarity.

where $\delta(t) \equiv \omega_{01} - \omega_d(t)$ represents the detuning, $\lambda = g_{12}/g_{01} = \sqrt{2}$ and $\alpha \equiv \omega_{12} - \omega_{01}$ is the anharmonicity, are shown to cancel the leakage to the second excited state [11]. These conditions can be converted into the current pulse parameters by:

$$\Omega(t) = \sqrt{\mathcal{E}_x^2(t) + \mathcal{E}_y^2(t)}, \tag{11a}$$

$$\Phi(t) = -\arctan\frac{\mathcal{E}_y(t)\cos\delta(t)t + \mathcal{E}_x(t)\sin\delta(t)t}{\mathcal{E}_x(t)\cos\delta(t)t - \mathcal{E}_y(t)\sin\delta(t)t}. \tag{11b}$$

Knowing this, the following probe contours can be considered:

$$\mathcal{E}_G = \left\{A\exp\left[-\frac{(t - t_g/2)^2}{2\sigma^2}\right] - B\right\}, \tag{12a}$$

$$\mathcal{E}_T = \left\{A\left[\tanh\left(\frac{t}{\sigma}\right) - \tanh\left(\frac{t - t_g}{\sigma}\right)\right] - B\right\}, \tag{12b}$$

$$\mathcal{E}_{SP} = \begin{cases} A\sin^2\left(\dfrac{\pi t}{2\sigma}\right), & t < \sigma \\ A, & \sigma \le t \le t_g - \sigma \\ A\sin^2\left(\dfrac{\pi(t_g - t)}{2\sigma}\right), & t > t_g - \sigma \end{cases}, \tag{12c}$$

being the gate time (t_g) and the σ parameter fixed, B a constant that sets the pulse to zero at $t = 0$ and $t = t_g$, and A a parameter that must be optimized so that the pulses implement the right amount of 0-1 rotation. This is performed here by the secant method. Figure A.1 in the Appendix shows the optimization results for A, and figure A.2 in the appendix provides an example of DRAG population evolution.

$\mathcal{E}_G$ and $\mathcal{E}_T$ [11] are Gaussian and tangential contours, whereas $\mathcal{E}_{SP}$ is a sine-plateau function that ascends and

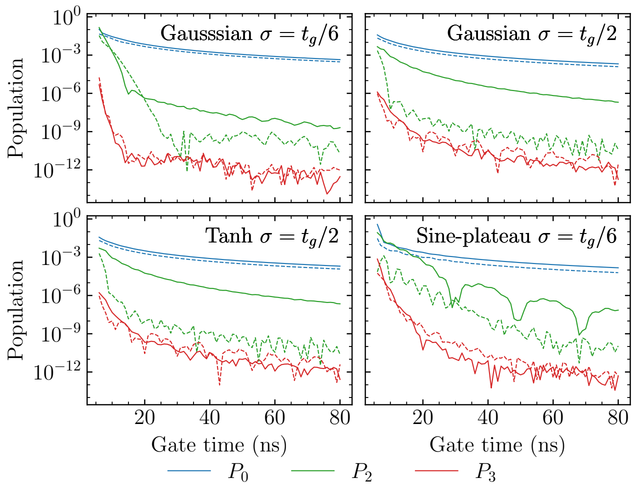

FIG. 2: Populations as function of gate time for different pulse profiles. Solid lines: envelopes Ω shaped as in (12) and $\Phi = 0$. Dashed lines: pulses prepared according to the DRAG protocol with $\mathcal{E}_x$ shaped as in Eq. (12). $1 - P_1$ practically coincides with P_0, as a sign of good performance avoiding population in level 2.

descends in a time $\sigma \le t_g/2$, but stays constant in between. The DRAG protocol can be tested by producing a pulse shape by means of Eq. (10) and (11), after having set $\mathcal{E}_x$ equal to any of the probe contours above.

Figure 2 shows that in all cases the amount of $|0\rangle$ population on gate termination is slightly reduced by the DRAG protocol, but even more significant is the reduction of the $|2\rangle$ population, which can be by a factor of up to 10^4. In the case of qutrit control this has an obvious application to perform a 0-1 rotation to prepare either the state $|1\rangle$ or a superposition of $|0\rangle$ and $|1\rangle$, remaining in the qutrit subspace. This would be achieved by optimizing A so that the right amount of rotation is implemented.

B. STIRAP protocol

Stimulated Raman Adiabatic Passage (STIRAP) is a technique widely used in quantum technologies [13, 14] that has been proved effective in quantum computation [15, 16]. It consists in the application of two pulses with envelopes Ω_1 and Ω_2 in resonance with the 0-1 and 1-2 transitions, respectively. The Hamiltonian whose interaction term $\mathcal{H}_I$ considers exclusively the coupling of each pulse with the transition with which it is resonant,

$$\mathcal{H}_I = \hbar \sum_{i=0,1} g_{i,i+1}\Omega_{i,i+1}(t)\cos(\omega_{i,i+1}t)\Pi_{i,i+1}, \qquad (13)$$

has the dark state $|D\rangle = \cos\Theta\,|0\rangle - \sin\Theta\,|2\rangle$ as a zero-eigenvalue eigenstate, with $\tan\Theta \equiv \Omega_{01}(t)/\Omega_{12}(t)$ [15]. By letting $\tan\Theta$ go from zero to infinity throughout the gate, a transfer of population between the $|0\rangle$ and $|2\rangle$ states occurs. This can be done through Gaussian pulses, separated by a time t_s:

$$\Omega_{i,i+1}(t) = A\exp\left[\frac{(t-\mu_{i,i+1})^2}{2\sigma^2}\right],\ \mu_{12} = \mu_{01} - t_s, \qquad (14)$$

where μ_{12} and μ_{01} denote the pulse centers and the amplitude A and the standard deviation σ are taken to be equal in both pulses. The counter-intuitive sequence, i.e. the application of the resonant 1-2 pulse in the first place and then the resonant 0-1 pulse ($t_s > 0$), leads to remarkable results [15–17]. The tuning is at all times undertaken slowly and if the global adiabatic condition [18],

$$\sqrt{2}At_s \gg 1, \qquad (15)$$

is fulfilled, no instantaneous $|1\rangle$ population will exist in the system in the course of the gate.

Nonetheless, in our particular scenario for the 4-level system, for consistency with the formalism presented, two interaction Hamiltonian terms $\mathcal{H}_{I,k}$ ($k = 0, 1$) are considered, where the two pulses interact non-resonantly with all the transitions:

$$\mathcal{H}_{I,k} = \hbar \sum_{i<j}^{3} g_{ij}\Omega_{k,k+1}(t)\cos^{a_{ij}}(\omega_{k,k+1}t)\Pi_{ij}. \qquad (16)$$

In the case of independent couplings, the adiabatic condition (15) can be fulfilled by freely increasing the amplitude A. However, in the non-resonant interaction frame, failing to keep A small enough would result into an intensification of this non-resonant effect, provoking a rapid oscillation in the populations, as seen in figure A.3.

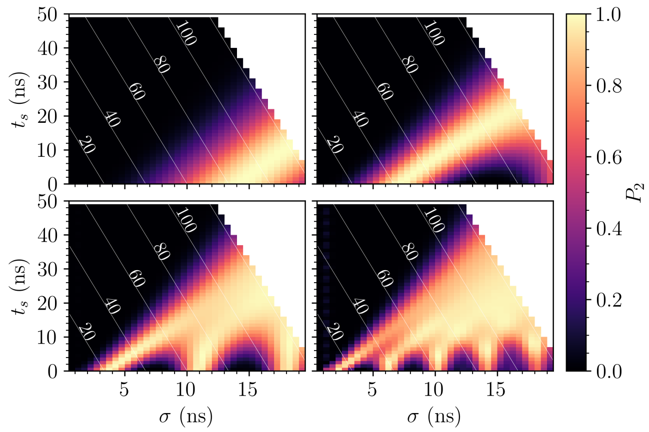

FIG. 3: Final population of the $|2\rangle$ state at STIRAP protocol termination for different σ and t_s, with amplitudes $A = 2\pi \times 20$ MHz and $2\pi\times 40$ MHz (top), $2\pi\times 80$ MHz and $2\pi\times 150$ MHz (bottom). Oblique lines with gate times (ns) $t_g = t_s + 6\sigma$ have been included for reference.

A compromise is achieved by letting A be small enough so that Eq. (16) can be approximated by (13), but large enough so that the condition (15) is fulfilled with times that are short enough so as not to observe decoherence. Final P_2 for varying parameters are shown in figure 3.

C. Pulse sequence

A straightforward approach to prepare a specific rotation is to implement a pulse sequence. A first pulse of length t_1, resonant with the 0-1 rotation, prepares the population of the $|0\rangle$ state to the desired value. Afterwards, a pulse of length t_2, being resonant with the 1-2 rotation, adjusts the ratio P_1/P_2.

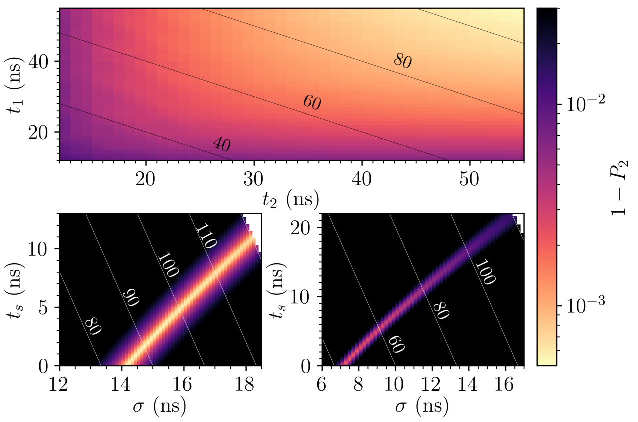

FIG. 4: $1-P_2$ at gate termination. Comparison of pulse sequence and STIRAP. Top: pulse sequence of $t_g = t_1 + t_2$, where the first pulse is Gaussian-DRAG with $t_1/\sigma = 2$ and the second one is Gaussian with $t_2/\sigma = 2$. The amplitudes are the ones that minimize P_0 in the DRAG pulse (figure A.1) and maximize P_2 in the second pulse. Bottom: STIRAP protocol at $A = 2\pi \times 20\,\text{MHz}$ (left) and $A = 2\pi \times 40\,\text{MHz}$ (right). t_g (ns) lines are shown for reference.

Figure 4 presents the results when the goal is the state $|2\rangle$. It can be seen there how the $|2\rangle$ population can be refined by enlarging the gate time t_1 of a first DRAG gate, and the gate time t_2 of a second Gaussian pulse. The comparison with the STIRAP simulated in the non-resonant frame shows how a pulse sequence is able to give similar results in smaller gate times.

IV. EFFECTIVE CHIRP PULSE

In the last section, we explore the effect of an effective time-dependent frequency ω_{eff} controlled by the phase $\Phi(t)$. The cosine argument of equation (6) is then:

$$\omega_d t + \Phi(t) \equiv \omega_{\text{eff}}(t)t; \quad \Phi(t) = (\omega_{\text{eff}}(t) - \omega_d)\, t \tag{17}$$

Knowing this, an effective frequency ω_{eff} is suggested, such that two differentiated phase regions come into play, where in each one only a single transition is resonantly excited—first the 0-1 and then the 1-2:

$$\omega_{\text{eff}}(t) = \frac{\omega_{12} - \omega_{01}}{2} \tanh\left(\frac{t-\mu}{\sigma}\right) + \frac{\omega_{12} + \omega_{01}}{2}, \tag{18}$$

where μ and σ are parameters to optimize that account for the position and width of the region transit. Thus, $\omega_{\text{eff}}(t \ll \mu) = \omega_{01}$ and $\omega_{\text{eff}}(t \gg \mu) = \omega_{12}$.

An envelope $\Omega(t)$ is also needed. Similarly, two regions are considered, now with three region transits, since it must begin and end at $\Omega(0) = \Omega(t_g) = 0$:

$$\Omega(t) = \sum_{i=1}^{3} C_i \tanh\left(\frac{t - M_i}{\Sigma_i}\right), \tag{19}$$

with $C_1 = \Omega_1/2$, $C_2 = (\Omega_2 - \Omega_1)/2$ and $C_3 = -\Omega_2/2$, where $\Omega_{1,2}$ are the pulse amplitudes at the 1$^{\text{st}}$ and 2$^{\text{nd}}$ regions. M_i and Σ_i are the position and width of the region transits.

All transit widths are set to $\sigma = \Sigma_i = 1.2\,\text{ns}$, and the envelope starts and is cut off at $|t - M_i| = 3\Sigma_i$, establishing $M_1 = 3\Sigma$ and $M_3 = t_g - 3\Sigma$. Parameters Ω_1, Ω_2, μ and M_2 are then optimized through the minimization of a cost function f by means of the Powell algorithm [19].

$$f = \frac{1}{3} \sum_{i=0}^{2} |P_i^* - \langle \Psi_{\mathcal{E}} | \Pi_i | \Psi_{\mathcal{E}} \rangle|, \tag{20}$$

where P_i^* denotes the target i-th state population and $|\Psi_{\mathcal{E}}\rangle$ denotes the system wave function after a pulse with Ω and Φ constructed as explained above, with $\omega_d = \omega_{01}$.

The robustness of the gate $1-\Delta$ is measured using:

$$1 - \Delta = 1 - \sqrt{\sum_{i=1,2} \left[(f_i^+ - f^*)^2 + (f_i^- - f^*)^2\right]} \tag{21}$$

where f^* denotes the minimum value obtained for the cost function and $f_i^{\pm}$ is the value of the cost function computed with the parameters that minimize it, except for Ω_i, whose value is $\Omega_i \pm \delta\Omega_i$. $\delta\Omega_i/\Omega_i = 5\%$ to emulate a slight deviation of the amplitudes during the evolution.

t_g (ns)	P_0^*	P_1^*	P_2^*	$1-f^*$	$1-\Delta$	Maximum P_3
20	1/3	1/3	1/3	0.99800	0.961	1.98×10^{-2}
18	1/2	1/4	1/4	0.99481	0.976	2.32×10^{-2}
16	1/10	4/5	1/10	0.99809	0.988	1.02×10^{-2}
20	3/10	0	7/10	0.99502	0.977	6.21×10^{-2}
30	1/3	1/3	1/3	0.99994	0.952	2.30×10^{-3}
	1/2	1/4	1/4	0.99998	0.959	1.38×10^{-3}
	1/10	4/5	1/10	0.99984	0.969	7.81×10^{-4}
	3/10	0	7/10	0.99997	0.959	1.21×10^{-3}

TABLE I: Optimization results for various target populations, with t_g of 30 ns and the lowest possible for each case.

Table I shows the results of the optimizations for various target populations. Their evolutions are shown in figures A.6 and A.7. $1-f^*$ is used as a fidelity marker, and acceptable results are obtained: up to 99.998% for a t_g of 30 ns, and above 99.4% for the lowest t_g obtained for each case (16 to 20 ns). If the target $|2\rangle$-state population is non-null, high Ω_1 are allowed since although non-resonant 1-2 rotation occurs in the first region, this is later corrected with the Ω_2 value.

These gate times, of course, must meet the experimental requirements of pulse generator time step and low-pass filtering, resulting from a potential opaqueness of certain electronic components to high frequencies.

V. CONCLUSIONS

Several techniques to induce specific qutrit populations in a superconducting transmon device have been discussed. They have at all times been achieved within gate times short enough so as not to consider decoherence, whose characteristic times are two to three orders of magnitude greater than the gate times used.

First, the DRAG technique has been introduced, which has shown to be able purify the preparation of the $|1\rangle$ state. This technique reduces the population of the $|2\rangle$ state by a factor of 10^2 to 10^4. This allows for the usage of the qutrit as a qubit when required.

Next, the STIRAP protocol has been discussed to prepare the $|2\rangle$ state, accompanied by a critical analysis of the case when the experimental setting requires the non-resonant coupling of the pulses with all transitions. A comparison with a slow pulse sequence has showed that preparing the system by parts yields equally good and faster results than the STIRAP protocol under the aforementioned restriction. Via a pulse sequence, a state $|2\rangle$ population of over 0.998 can be prepared in 60 ns.

Finally, a new effective-chirp pulse technique is suggested. By means of it, arbitrary qutrit populations can be reached in very short gate times –16 to 20 ns– with acceptable fidelity (up to 99.8%) and robustness. Thus, one may saturate the experimental possibilities of pulse generator time mesh and electronic opaqueness to high frequencies to freely populate the qutrit states.

Further work could be oriented towards the extension of the protocol such that it incorporates the ability to control the relative phases of the qutrit states. In that case, a true quantum gate that performed arbitrary rotations in the qutrit space would be designed.

Acknowledgments

I would like to warmly thank my supervisors Pol Forn (IFAE) and Sofyan Iblisdir (UB) for their continued care and advice, and also Artur García (BSC) for his aid in optimization techniques. Many thanks to Jordi Mompart and Verònica Ahufinger (UAB) for sharing their time and knowledge on the STIRAP technique. Finally, I would like to thank the Quantic team (UB/BSC) and the Quantum Computing Technology team (IFAE) for their interest and enthusiasm along the months of my stay there, especially David López and Adrián Pérez.

[1] Deutsch, D. E., "Quantum computational networks," *Proc. R. Soc. Lond. A*, **425**: 73 (1989).

[2] Bullock, S. S. et al., "Asymptotically optimal quantum circuits for d-level systems," *Phys. Rev. Lett.*, **94**: 230502 (2005).

[3] Schirmer, S. et al., "Implementation of controlled multi-qudit operations for a solid-state quantum computer based on charge qudits," *arXiv preprint quant-ph/0305052*, (2003).

[4] Bartlett, S. D. et al., "Quantum encodings in spin systems and harmonic oscillators," *Phys. Rev. A*, **65**: 052316 (2002).

[5] Shapiro, E. et al., "Strong-field molecular alignment for quantum logic and quantum control," *Phys. Rev. A*, **67**: 013406 (2003).

[6] Koch, J. et al., "Charge-insensitive qubit design derived from the Cooper pair box," *Phys. Rev. A*, **76**: 042319 (2007).

[7] Makhlin, Y. et al., "Quantum-state engineering with Josephson-junction devices," *Rev. Mod. Phys.*, **73**: 357 (2001).

[8] Johansson, J. R. et al., "QuTiP 2: A Python framework for the dynamics of open quantum systems," *Comput. Phys. Commun.*, **184**: 1234 (2013).

[9] Foot, C. J. et al., "Atomic physics," *Oxford University Press*, **7** (2005).

[10] Yurtalan, M. A. et al., "Implementation of a Walsh-Hadamard gate in a superconducting qutrit," *arXiv preprint arXiv:2003.04879*, (2020).

[11] Motzoi, F. et al., "Simple pulses for elimination of leakage in weakly nonlinear qubits," *Phys. Rev. Lett.*, **103**: 110501 (2009).

[12] Chow, J. M. et al., "Optimized driving of superconducting artificial atoms for improved single-qubit gates," *Phys. Rev. A*, **82**: 040305 (2010).

[13] Bergmann, K. et al., "Coherent population transfer among quantum states of atoms and molecules," *Reviews of Modern Physics*, **70**: 1003 (1998).

[14] Vitanov, N. V. et al., "Laser-induced population transfer by adiabatic passage techniques," *Annu. Rev. Phys. Chem.*, **52**: 763 (2001).

[15] Kumar, K. et al., "Stimulated Raman adiabatic passage in a three-level superconducting circuit," *Nat. Commun.*, **7**: 10628 (2016).

[16] Xu, H. et al., "Coherent population transfer between uncoupled or weakly coupled states in ladder-type superconducting qutrits," *Nat. Commun.*, **7**: 1 (2016).

[17] Vepsäläinen, A. et al., "Superadiabatic population transfer in a three-level superconducting circuit," *Sci. Adv.*, **5**: eaau5999 (2019).

[18] Panda, C. D. et al., "Stimulated Raman adiabatic passage preparation of a coherent superposition of ThO H 3 Δ 1 states for an improved electron electric-dipole-moment measurement," *Phys. Rev. A*, **93**: 052110 (2016).

[19] Powell, M. J., "Direct search algorithms for optimization calculations," *Acta Numer.*, **7**: 287 (1998).

[20] Luque Merino, R., "Coherent control of a superconducting quantum bit," Master thesis, Quantic Group, Universitat Politècnica de Catalunya (2019).

[21] They are strictly forbidden in the harmonic oscillator [9], but still heavily unprivileged in the transmon modified energy levels.

VI. APPENDIX

A. Device parameters

Parameter	Value
0-1 transition frequency (ω_{01})	$2\pi \times 4.89\,\mathrm{GHz}$
1-2 transition frequency (ω_{12})	$2\pi \times 4.58\,\mathrm{GHz}$
0-2 transition frequency ($\omega_{02}/2$)	$2\pi \times 4.74\,\mathrm{GHz}$
0-3 transition frequency (ω_{03})	$2\pi \times 13.75\,\mathrm{GHz}$
1-3 transition frequency ($\omega_{13}/2$)	$2\pi \times 4.43\,\mathrm{GHz}$
2-3 transition frequency (ω_{23})	$2\pi \times 4.28\,\mathrm{GHz}$
Anharmonicity (α)	$-2\pi \times 306\,\mathrm{MHz}$
Relative anharmonicity (α_r)	-6.25×10^{-2}
Charing energy ($E_C/\hbar$)	$2\pi \times 306\,\mathrm{MHz}$
Josephson energy ($E_J/\hbar$)	$2\pi \times 11.04\,\mathrm{GHz}$

TABLE A.I: Experimental parameters of the transmon device [20] (updated). 0-1 and 1-2 transition frequencies were measured whereas the rest of parameters were computed using Eqs. (2) and (1). Notice that the two-photon processes are modelled with a frequency that corresponds to half the energy difference between levels. Relative anharmonicity is computed as $\alpha_r = \alpha/\omega_{01}$.

B. Optimization results

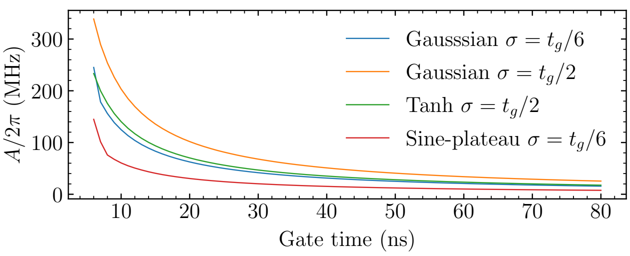

FIG. A.1: Optimal A-parameters of Eq. (12) to performe a π-pulse and prepare state $|1\rangle$ for both DRAG and non-DRAG sequences, since both values practically coincide.

t_g (ns)	P_0^*	P_1^*	P_2^*	$\Omega_1/2\pi$ (MHz)	$\Omega_2/2\pi$ (MHz)	μ (ns)	M_2 (ns)
20	1/3	1/3	1/3	71.305	70.620	12.472	12.938
18	1/2	1/4	1/4	74.463	9.023	9.023	8.957
16	1/10	4/5	1/10	103.439	10.929	10.929	7.150
20	3/10	0	7/10	114.933	9.787	8.787	6.864
30	1/3	1/3	1/3	34.193	21.535	15.000	14.877
	1/2	1/4	1/4	27.196	21.268	15.000	15.001
	1/10	4/5	1/10	32.367	10.988	18.760	18.674
	3/10	0	7/10	35.440	41.510	15.102	15.482

TABLE A.II: Optimal parameters found for the results presented in table I and figures A.6 and A.7.

C. Population evolutions

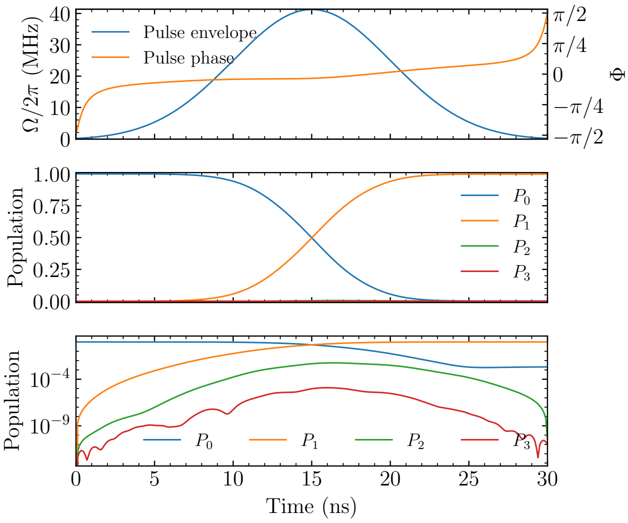

FIG. A.2: Population evolution in the preparation of the $|1\rangle$ state via the DRAG protocol with $t_g = 30\,\mathrm{ns}$, $\sigma = t_g/6$. Pulse envelope and phase are shown, along with the population of each of the states, in linear and logarithmic plots.

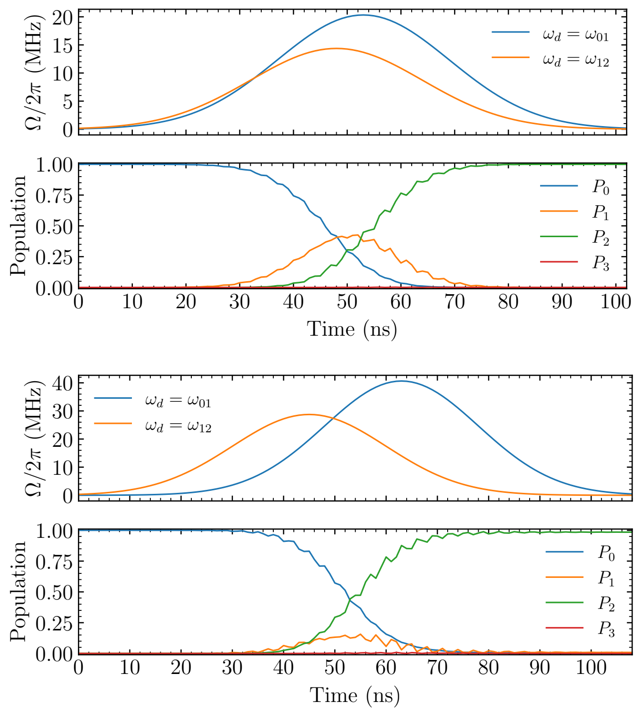

FIG. A.3: Pulses and populations evolution in the preparation of the $|2\rangle$ state via the STIRAP protocol. Top: $A = 2\pi \times 20\,\mathrm{MHz}$, $\sigma = 16\,\mathrm{ns}$, $t_s = 5\,\mathrm{ns}$. Bottom: $A = 2\pi \times 40\,\mathrm{MHz}$, $\sigma = 15\,\mathrm{ns}$, $t_s = 18\,\mathrm{ns}$. The envelopes are scaled by a factor so $A = g_{01}\Omega_{01}(\mu_{01}) = g_{12}\Omega_{12}(\mu_{12})$: see Eqs. (16) and (14).

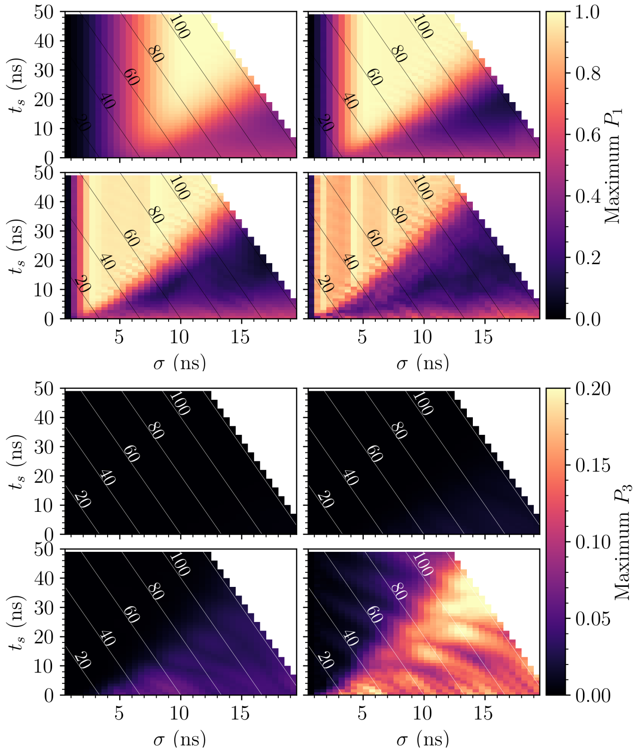

FIG. A.4: Maximum population of the $|1\rangle$ and $|3\rangle$ states during the STIRAP protocol with amplitudes $A = 2\pi \times 20\,\mathrm{MHz}$ and $2\pi \times 40\,\mathrm{MHz}$ (top), $2\pi \times 80\,\mathrm{MHz}$ and $2\pi \times 150\,\mathrm{MHz}$ (bottom). Oblique lines with gate times (ns) $t_g = t_s + 6\sigma$ have been included for reference.

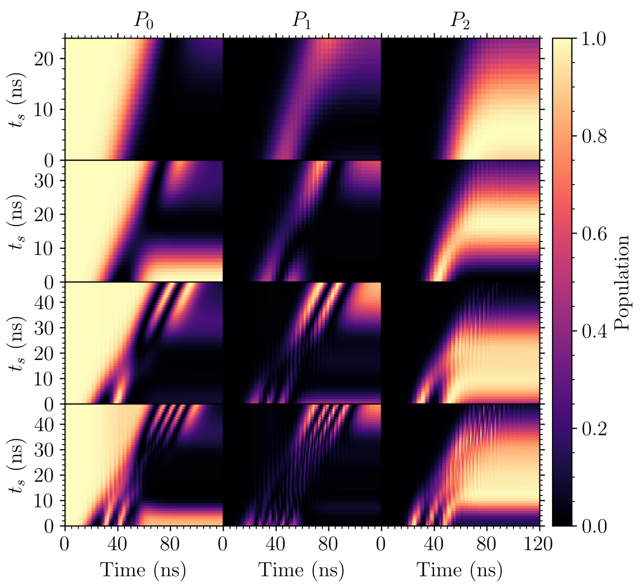

FIG. A.5: Evolution of the population in the $|0\rangle$, $|1\rangle$ and $|2\rangle$ states throughout the STIRAP protocol for varying separations. Top to bottom: $A = 2\pi \times 20\,\mathrm{MHz}$, $\sigma = 16\,\mathrm{ns}$; $A = 2\pi \times 40\,\mathrm{MHz}$, $\sigma = 14\,\mathrm{ns}$; $A = 2\pi \times 80\,\mathrm{MHz}$, $\sigma = 12\,\mathrm{ns}$; and $A = 2\pi \times 150\,\mathrm{MHz}$, $\sigma = 12\,\mathrm{ns}$.

Figure A.2 shows the system evolution in the preparation of the $|1\rangle$-state via a 30 ns DRAG gate with $\sigma = t_g/6$.

Figure A.3 shows the system evolution in the preparation of the $|2\rangle$-state via the STIRAP protocol with $A = 2\pi \times 20\,\mathrm{MHz}$ and $A = 2\pi \times 40\,\mathrm{MHz}$. The quality of the state $|2\rangle$ achieved is better in the case of the lower-magnitude pulse than for the higher-magnitude one: 99.94% vs. 98.50%. This is due to the fact that a lower Rabi frequency reduces the non-resonant effect.

On the other hand, as discussed in section III B, since the adiabatic condition (15) is better fulfilled for higher-magnitude pulses, the maximum P_1 along the gate is lower in the stronger pulse: 16% vs 43%. This becomes especially relevant when this technique is intended to prepare a superposition of the $|0\rangle$ and the $|2\rangle$ pulses. This is also reflected in figure A.4a. Below, figure A.4b shows how greater Rabi frequencies result in a relevant leakage to the $|3\rangle$ state, making them unacceptable.

Figure A.5 shows the evolution of the qutrit populations under the STIRAP protocol for increasing Rabi frequencies. It can be seen that, for intense pulses, the out-of-resonance effect produces undesirable rapid oscillations during the transition to the $|2\rangle$ state.

Finally, figures A.6 and A.7 show the system evolution in the preparation of various target states, namely $(P_0^*, P_1^*, P_2^*) = (1/3, 1/3, 1/3)$, $(1/2, 1/4, 1/4)$, $(1/10, 4/5, 1/10)$ and $(3/10, 0, 7/10)$, with the effective-chirp protocol. The pulse parameters are given in table A.II, and the results in table I. The 30 ns gate yields very good results, but shorter gate times are also possible. The shortest it is possible to achieve before losing fidelity depends on the target populations nature.

Since $(1/10, 4/5, 1/10)$ resembles a 0-1 transition, it can be produced in shorter gate times –16 ns–. The still little amount of $|2\rangle$-state population in $(1/2, 1/4, 1/4)$ enables this set of populations to be prepared in 18 ns. However, the 1-2 rotation must be undertaken more carefully since, as table A.I shows, undesired transitions to the $|3\rangle$ state are close to ω_{12}. Consequently, the fact that $(1/3, 1/3, 1/3)$ and $(3/10, 0, 7/10)$ require more 1-2 rotation demands slightly longer gate times: 20 ns.

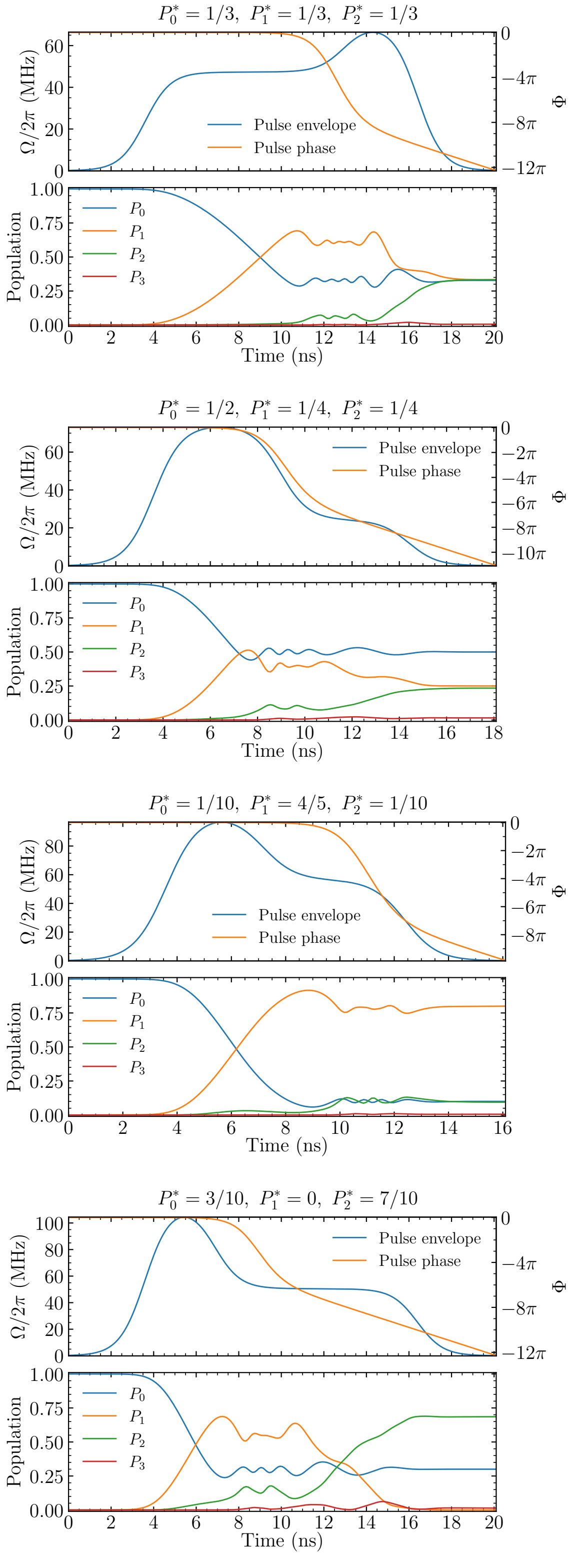

FIG. A.6: Evolution of the populations for the chirp preparation of the final state with different target populations in the lowest time possible for each.

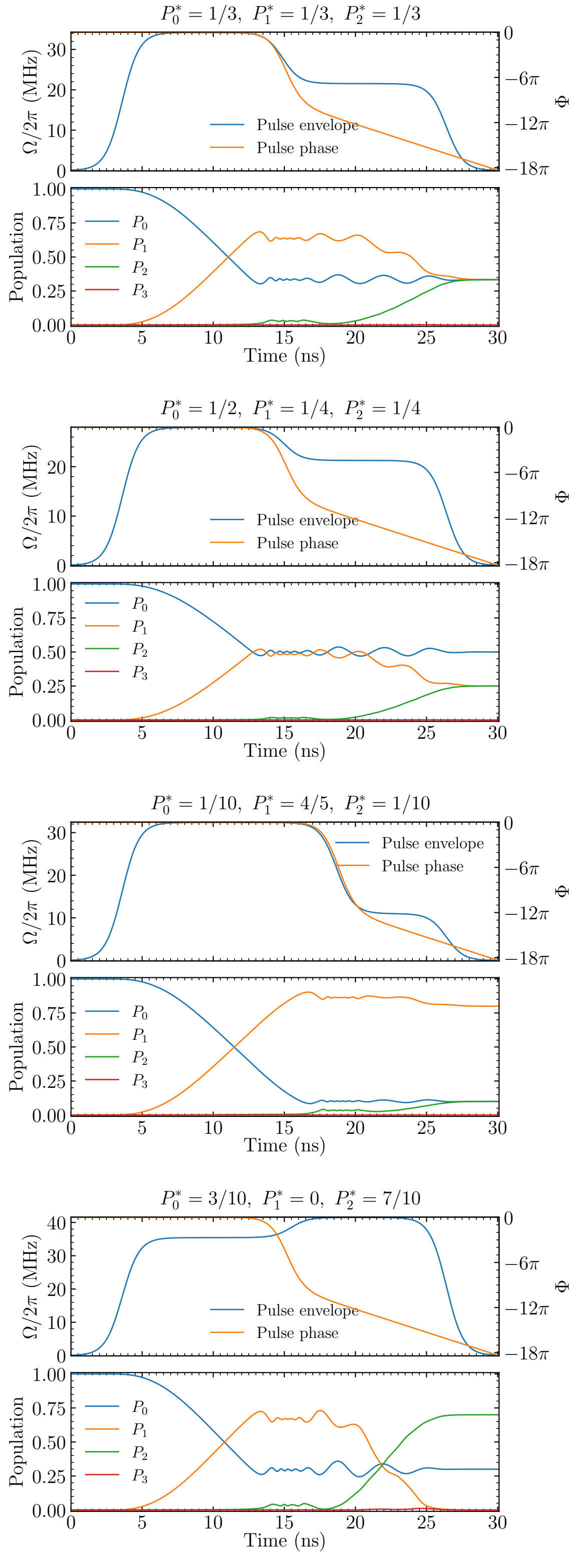

FIG. A.7: Evolution of the populations for the chirp preparation of the final state with different target populations in 30 ns.